Steady-State Upscaling of Polymer Flooding

S. T. Hilden* (NTNU/SINTEF) K.A. Lie (SINTEF) X. Raynaud (SINTEF)

Abstract

Upscaling of parameters involved in single and two-phase flow has been researched quite extensively, and several methods for performing upscaling are known and understood. Less work has been done related to upscaling of enhanced oil recovery simulations. This is what we investigate, and in particular, we consider upscaling of parameters related to polymer flooding, which is the process in which large polymer molecules are added to the injected water to enhance its ability to push hydrocarbons through the reservoir. Herein, the polymer flooding process is described as a two-phase, immiscible system that in addition to a Todd–Longstaff mixing model includes permeability reduction, polymer adsorption, and dead pore space.

Effective parameters are computed by running simulations until a steady-state is reached and then performing upscaling based on the fluxes. This method is used by a major oil company as part of an established work flow for single and two-phase upscaling, and it is therefore natural to try to extend the method to polymer flooding. The upscaling is performed on the meter scale, where the steady-state assumption best can be justified. The procedure involves first performing single-phase upscaling of the absolute permeability, then two-phase upscaling of relative permeabilities, and finally, upscaling of the parameters involved in polymer flooding. The new upscaling method is verified against an analytical solution and validated on two synthetic models that include real data.

Results show that the permeability reduction factor, which only depends on polymer concentration in the fine-scale model, will generally also depend on water saturation in the upscaled model. This introduces addition computational costs in the simulation, since the property evaluations now require extensive use of lookup-tables and interpolation. We therefore suggest making simplifications in order to reduce the complexity.

Introduction

Upscaling of single and two-phase flow has been researched quite extensively, and several methods for performing upscaling is known and understood (see e.g., Christie (2001) for an overview and an extensive list of relevant references). Upscaling of enhanced oil recovery processes is much less researched. Herein, we investigate upscaling of parameters related to polymer flooding. Polymer flooding is the process in which water-soluble polymers are added to the water before it is injected into the reservoir. The purpose of the polymer is to increase the viscosity of the water, which will lower the mobility of the displacement front and thus increase sweep efficiency. Adsorption of polymer molecules onto the rock surface will reduce the permeability, but also dilute the polymer concentration and reduce the EOR effect. At the same time, smaller portions of the pore space may be inaccessible to the water-polymer mixture since the polymer molecules are too large to enter small pore throats. See Lake (2010) for a more thorough discussion.

The purpose of our work is to develop an upscaling method for polymer flow physics on the meter scale. Steady-state upscaling relies on the assumption that the flow in the region of interest is close to a steady state, which on the meter scale is a reasonable assumption away from wells. Steady-state methods are already used by a major oil company as part of an established work flow for single and two-phase upscaling, and it is therefore natural to try to extend this method to polymer flooding. Assuming steady state will enable us to simplify the flow model by disregarding time-dependent terms and develop a simple, sequential upscaling procedure that consists of first performing single-phase upscaling of absolute permeability, then two-phase upscaling of relative permeabilities, and finally, upscaling of the parameters involved in polymer flooding.

Mathematical Model

The model considered is an extension of the black-oil model for oil and water, where in addition to the oil and water saturations, s_o and s_w, we have the concentration c_p of polymer as a primary unknown. The concentration is given in units of mass per volume of water. It is assumed that the presence of polymer changes the water viscosity, but does not influence the oil phase. The conservation equations for oil, water, and water with polymer are

$$\frac{\partial}{\partial t}\left(\frac{\phi s_o}{B_o}\right)+\nabla\cdot\left(\frac{v_o}{B_o}\right)=0, \tag{1a}$$

$$\frac{\partial}{\partial t}\left(\frac{\phi s_w}{B_w}\right)+\nabla\cdot\left(\frac{v_w}{B_w}\right)=0, \tag{1b}$$

$$\frac{\partial}{\partial t}\left(\frac{\phi(1-s_{\mathrm{dpv}})s_w c_p}{B_w}\right)+\frac{\partial}{\partial t}\left(\rho_r c_a(1-\phi_{\mathrm{ref}})\right)+\nabla\cdot\left(\frac{c_p v_p}{B_w}\right)=0, \tag{1c}$$

with the closing relation $s_w+s_o=1$ and fluxes given as

$$v_o=-\frac{k_{ro}}{\mu_o}K\left(\nabla p_o-\rho_o g\nabla z\right), \tag{2a}$$

$$v_w=-\frac{k_{rw}}{\mu_{w,\mathrm{eff}}R_k}K\left(\nabla p_w-\rho_w g\nabla z\right), \tag{2b}$$

$$v_p=-\frac{k_{rw}}{\mu_{p,\mathrm{eff}}R_k}K\left(\nabla p_w-\rho_w g\nabla z\right). \tag{2c}$$

The porosity ϕ, absolute permeability K, phase pressures p_α, fluid densities ρ_α, and formation volume factors B_α are familiar from the two-phase black-oil equations. In addition, there are parameters related to the polymer: R_k is the relative-permeability reduction factor, s_{dpv} denotes the dead pore space, c_a is the amount of polymer adsorbed on the rock face, ρ_r is the rock density, and ϕ_{ref} a reference porosity. The polymer effects are described in more detail below.

The effective viscosities of pure water and water with polymer are denoted $\mu_{w,\mathrm{eff}}$ and $\mu_{p,\mathrm{eff}}$, respectively.

These effective viscosities are defined using the Todd–Longstaff mixing model (Todd and Longstaff, 1972). The viscosity of a fully mixed solution of water and polymer is denoted $\mu_m(c_p)$, and the effective polymer viscosity is given by

$$\mu_{p,\text{eff}} = \mu_m(c_p)^{\omega}\mu_m(c_{p,\max})^{1-\omega},$$

where $c_{p,\max}$ is the maximum possible polymer concentration, and $\omega \in [0,1]$ is the Todd–Longstaff mixing parameter. The mixing parameter is equal one when the polymer solution and water are fully mixed, whereas $\omega = 0$ if the polymer solution is completely segregated from the water. In a similar way, the viscosity of partially mixed water is defined as

$$\mu_{w,e} = \mu_m(c_p)^{\omega}\mu_w^{1-\omega}.$$

The effective water viscosity $\mu_{w,\text{eff}}$ is then given by

$$\frac{1}{\mu_{w,\text{eff}}} = \frac{1 - c_p/c_{p,\max}}{\mu_{w,e}} + \frac{c_p/c_{p,\max}}{\mu_{p,\text{eff}}}.$$

Polymer molecules are relatively large and a portion of the pore volume may therefore be inaccessible to the polymer, which again may result in an accelerated polymer flow. This effect is modeled by the dead pore space s_{dpv}.

Adsorption is the effect of polymer molecules attaching to the rock surface. Adsorption will cause the polymer concentration to decrease, and consequently so will the viscosity. The adsorption function $c_a(c_p)$ gives the relationship between the polymer concentration and the amount of adsorbed polymer. The adsorption of polymer may reduce the relative permeability, which is modeled by the reduction factor R_k, defined by

$$R_k(c_p) = 1 + (\text{RRF} - 1)\,\frac{c_a(c_p)}{c_{a,\max}}, \tag{3}$$

where $\text{RRF} \geq 1$ is called the residual resistance factor and $c_{a,\max}$ is the maximum adsorption.

Equations at Steady State

In the following, we ignore compressibility to simplify notation, but this may easily be included without changing the conclusions. At steady state, there is no time dependency in the system, and so (1) reduces to the steady-state equations

$$\nabla \cdot v_o = 0, \quad \nabla \cdot v_w = 0, \quad \nabla \cdot (c_p v_p) = 0, \tag{4}$$

where the fluxes are given by (2). By defining the function

$$f(c_p) = c_p \frac{\mu_{w,\text{eff}}}{\mu_{p,\text{eff}}},$$

we have the relation $c_p v_p = f(c_p) v_w$. Then the polymer steady-state equation reads

$$\nabla \cdot (c_p v_p) = \nabla \cdot \Big(f(c_p) v_w \Big) = \left(\frac{\partial f(c_p)}{\partial c_p} \nabla c_p \right) \cdot v_w + f(c_p) \Big(\nabla \cdot v_w \Big) = 0.$$

From (4) it follows that $\nabla \cdot v_w = 0$, and hence we are left with

$$\left(\frac{\partial f(c_p)}{\partial c_p} \nabla c_p \right) \cdot v_w = 0. \tag{5}$$

It can be shown that $f'(c_p) > 0$ for all $c_p \in [0, c_{p,\max}]$. As the water flux at steady state in general will be nonzero, Equation (5) implies that $\nabla c_p = 0$. That is, the polymer concentration is constant at steady state. Notice, however, that this constant may jump to a different value across any interface with zero

water flux that isolates parts of the global domain into separate flow systems. We will in the following assume that there are no such interfaces in the interior of the domain during upscaling, and hence we can take the polymer concentration to be constant at steady state. A consequence of this assumption, is that the effective viscosities become proportional to the pure water viscosity. If the viscosity of a fully mixed solution can be written as $\mu_m(c_p) = \mu_{w,\text{mult}}(c_p)\mu_w$ for some function $\mu_{w,\text{eff}}$ dependent on c_p (this is the input form used in a leading commercial simulator), then a constant polymer concentration implies

$$\mu_{p,\text{eff}} = \mu_m(c_p)^\omega \mu_m(c_{p,\max})^{1-\omega} = \left[\mu_{w,\text{mult}}(c_p)^\omega \mu_{w,\text{mult}}(c_{p,\max})^{1-\omega}\right]\mu_w \doteq \alpha\mu_w$$

where α is constant. Introducing the shorthand notation $\bar{c}_p = c_p/c_{p,\max}$, the effective water viscosity is

$$\frac{1}{\mu_{w,\text{eff}}} = \frac{1-\bar{c}_p}{\mu_{w,e}} + \frac{\bar{c}_p}{\mu_{p,\text{eff}}} = \frac{1-\bar{c}_p}{\mu_m(c_p)^\omega \mu_w^{1-\omega}} + \frac{\bar{c}_p}{\alpha\mu_w} = \left[\frac{1-\bar{c}_p}{\mu_{w,\text{mult}}(c_p)^\omega} + \frac{\bar{c}_p}{\alpha}\right]\frac{1}{\mu_w} \doteq \frac{1}{\beta}\frac{1}{\mu_w}$$

and so $\mu_{w,\text{eff}} = \beta\mu_w$, where β is constant. Inserting these relations for effective viscosities into the steady-state equations (4), the water and polymer equations reduce to the same equation, and the system becomes essentially a two-phase system

$$\nabla\cdot\left(\frac{k_{ro}}{B_o\mu_o}K(\nabla p_o - \rho_o g\nabla z)\right) = 0, \tag{6a}$$

$$\nabla\cdot\left(\frac{\tilde{k}_{rw}}{B_w\mu_w}K(\nabla p_w - \rho_w g\nabla z)\right) = 0, \tag{6b}$$

where the altered water relative permeability is $\tilde{k}_{rw} = k_{rw}/R_k$, and R_k is given by (3).

Upscaling Methodology

Our upscaling procedure consists of sequentially applying single-phase upscaling of the absolute permeability, two-phase upscaling of relative permeabilities, before upscaling the parameters involved in polymer flooding. The single and two-phase methods we use for upscaling are described in several papers, see e.g., (Christie, 2001; Pickup et al., 2000). In the following, we will let superscript '$*$' denote an upscaled value (which may be scalar or tensor), so that e.g., K^* denotes the upscaled value of the permeability field K.

Single-Phase Upscaling

Flow-based upscaling of permeability depends on the choice of boundary conditions applied. We consider both fixed and periodic boundary conditions. Assume first that fixed boundary conditions are applied. Consider a domain Ω of the fine grid that is to be upscaled to a single coarse grid block Ω^c. For each direction $d = \{x,y,z\}$, a pressure drop Δp is applied across the domain Ω, and the pressure equation

$$\nabla\cdot(K\nabla p) = 0$$

is solved to obtain the flux field v_d. The average flux out of the domain is then

$$\bar{v}_d = \frac{1}{A_d}\int_{\partial\Omega_d} v_d\cdot n_d\, dA, \quad \text{where} \quad A_d = \int_{\partial\Omega_d} dA,$$

and $\partial\Omega_d$ denotes the boundary of Ω at the low pressure side in d-direction, and n_d is the normal vector to this boundary. The upscaled permeability in direction d is then given by

$$K^{*,d} = \frac{L_d}{\Delta p}\bar{v}_d = \frac{L_d}{\Delta p A_d}\int_{\partial\Omega_d} v_d\cdot n_d\, dA, \tag{7}$$

where L_d is a representative distance between the inflow and outflow boundaries. As this upscaling is performed in turn for each direction, the upscaled (absolute) permeability becomes a diagonal tensor

$$K^* = \text{diag}(K^{*,x}, K^{*,y}, K^{*,z}).$$

If periodic boundary conditions are chosen instead, the upscaled permeability becomes a full upscaled permeability tensor as cross-flow is included.

Capillary Limit Method

The assumptions of the capillary limit method is that the capillary forces have reached an equilibrium, and that capillary forces dominate such that viscous and gravitational forces may be neglected. This may be a valid assumption in regions of the reservoir in which the flow rate is very low. The method is described in the following steps:

i) Select a value $\hat{p}_{\text{cow}}$ of the capillary pressure.
ii) Invert the capillary pressure curve to obtain a saturation distribution $\hat{s}_w = p_{\text{cow}}^{-1}(\hat{p}_{\text{cow}})$.
iii) Compute the average water saturation s_w^* by pore volume averaging,

$$s_w^* = \frac{\int_\Omega \phi \hat{s}_w \, dV}{\int_\Omega \phi \, dV}. \tag{8}$$

iv) Set the absolute permeability in the domain equal to the permeability $\tilde{K}_w = k_{rw}(\hat{s}_w)K$ of the water phase. Then, for each direction $d = \{x, y, z\}$, perform a single-phase upscaling to obtain upscaled (effective) phase permeabilities $\tilde{K}_w^{*,d}$. In a similar fashion, obtain upscaled oil permeabilities $\tilde{K}_o^{*,d}$.
v) Compute the upscaled relative permeabilities from the equations

$$k_{rw}^{*,d}(s_w^*) = \frac{\tilde{K}_w^{*,d}}{K^{*,d}} \quad \text{and} \quad k_{ro}^{*,d}(s_w^*) = \frac{\tilde{K}_o^{*,d}}{K^{*,d}},$$

where $K^{*,d}$ is the upscale absolute permeability in the d-direction as given by (7).

This process is repeated for different values $\hat{p}_{\text{cow}}$ to obtain upscaled relative permeabilities for different values of s_w^*. As this upscaling is performed for each direction, we obtain an upscaled relative permeability curve for each of the three dimension. We do not consider full tensor upscaling of relative permeabilities.

Viscous Limit Method

The viscous limit method assumes that viscous forces dominate, and that capillary and gravitational forces may be neglected. This may be a valid assumption in regions of high flow. The basic steps of the method are as follows:

i) Select a value $\hat{f}_w$ of the fractional flow.
ii) Invert the fractional-flow curve to obtain a saturation distribution $\hat{s}_w = f_w^{-1}(\hat{f}_w)$.
iii) Compute the average water saturation s_w^* by pore volume averaging (8).
iv) Set the absolute permeability in the domain equal to the total mobility times the absolute permeability, such that

$$\tilde{K}_\lambda = \lambda_t(\hat{s}_w)K = \left(\frac{k_{rw}(\hat{s}_w)}{\mu_w} + \frac{k_{ro}(\hat{s}_w)}{\mu_o} \right) K,$$

and perform a single-phase upscaling for each direction $d = \{x, y, z\}$ to obtain upscaled $\tilde{K}_\lambda^{*,d}$.
v) Compute the upscaled relative permeabilities from the equations

$$k_{rw}^{*,d}(s_w^*) = \mu_w \hat{f}_w \frac{\tilde{K}_\lambda^{*,d}}{K^{*,d}} \quad \text{and} \quad k_{ro}^{*,d}(s_w^*) = \mu_o (1 - \hat{f}_w) \frac{\tilde{K}_\lambda^{*,d}}{K^{*,d}}.$$

Similar to the capillary limit method, this process is repeated for different values of the fractional flow $\hat{f}_w$ to obtain upscaled relative permeabilities for different values of s_w^*.

Flow Simulation

Without assuming neither the capillary or viscous limit, the saturation distribution at steady state may be found by performing a two-phase flow simulation. By applying a set of boundary conditions on the domain, a simulation is run until the change in saturation is below some set threshold. This method is obviously much more computationally expensive than the viscous and capillary limit methods. On the other hand, no assumptions have to be made about the dominating forces in the system.

For each direction $d = \{x, y, z\}$, perform the following steps:

i) Select a water saturation $\hat{s}_w$, and initialize the domain with saturation equal to $\hat{s}_w$ in all cells.
ii) Apply a pressure drop across the domain in the d-direction and run a two-phase simulation until the saturation change is below some prescribed threshold (one may also use a threshold for the fluxes).
iii) Compute the average water saturation s_w^* by pore volume averaging (8).
iv) Perform single-phase upscaling of the phase permeabilities $\tilde{K}_{w,d} = k_{rw}(\hat{s}_w)K$ and $\tilde{K}_{o,d} = k_{ro}(\hat{s}_w)K$.
v) Compute the upscaled relative permeabilities from the equations

$$k_{rw}^{*,d}(s_w^*) = \frac{\tilde{K}_w^{*,d}}{K^{*,d}} \quad \text{and} \quad k_{ro}^{*,d}(s_w^*) = \frac{\tilde{K}_o^{*,d}}{K^{*,d}}.$$

These steps are then repeated for different values of the saturation $\hat{s}_w$. As for the two other methods, we end up with a diagonal tensor representing the upscaled relative permeability for each phase.

Capillary Pressure Upscaling

In two phase flow, the capillary pressure also needs to be upscaled, in addition to the relative permeabilities. For this upscaling, we use a volume averaging, such that

$$p_{cow}^*(s_w^*) = \frac{\int_\Omega \phi\, p_{cow}(s_w)\, dV}{\int_\Omega \phi\, dV}.$$

Polymer Upscaling

If the polymer concentration is constant at steady state, the effective viscosities for water and water with polymer are proportional to the pure water viscosity and factor out of the steady-state equations (4). Hence, it is natural to neither perform an upscaling of $\mu_{w,\text{eff}}$ and $\mu_{p,\text{eff}}$ nor of the mixing parameter ω. On the other hand, as the reduced steady-state equations (6) have an altered water relative permeability $\tilde{k}_{rw} = k_{rw}/R_k$, the reduction factor R_k is considered a better candidate for upscaling.

Because the steady-state equations for polymer reduce to a two-phase system, we can apply the two-phase upscaling methods described above to achieve upscaled (effective) values for $\tilde{k}_{rw}^*$ and from these compute upscaled R_k^*. The upscaling procedure is described in the following:

i) Select a value $\hat{c}_p$ for the polymer concentration.
ii) Set the water relative permeability equal to $\tilde{k}_{rw} = k_{rw}/R_k(\hat{c}_p)$.
iii) Apply a two-phase upscaling method to get upscaled relative-permeability curves $\tilde{k}_{rw}^{*,d}$ for each dimension d.
iv) Compute the upscaled R_k^* from the equation

$$R_k^{*,d}(s_w^*, c_p^*) = \frac{k_{rw}^{*,d}(s_w^*)}{\tilde{k}_{rw}^{*,d}(s_w^*)},$$

where $c_p^* = \hat{c}_p$, as the concentration is constant, and $k_{rw}^{*,d}$ is the upscaled relative permeability for water.

These steps are repeated for different values of the polymer concentration $\hat{c}_p$.

The reduction factor R_k may vary with the rock types inside the coarse block Ω, and so the saturation distribution found using two-phase upscaling of $\tilde{k}_{rw} = k_{rw}/R_k$ will in general be different from the one found using k_{rw}. Because of this, the upscaled R_k^* will also depend on the upscaled water saturation s_w^*, in addition to depending on c_p^*. This happens even though the fine-scale R_k is only a function of c_p.

The adsorption function $c_a(c_p)$ is upscaled using standard volume averaging. As the amount of adsorbed polymer is related to the surface area of the rock, which again is related to the mass of the rock, we use

$$c_a^*(c_p^*) = \frac{\int_\Omega \rho_r(1-\phi)c_a(c_p)\,dV}{\int_\Omega \rho_r(1-\phi)\,dV}.$$

Numerical Experiments

The upscaling methods outlined above have been implemented using the Matlab Reservoir Simulation Toolbox (MRST; Lie et al., 2012), which is an open source toolbox for rapid prototyping of new computational methods for reservoir engineering. In our implementation, the dynamic flow simulations are performed using a fully-implicit solver, which is based on automatic differentiation and comes as a separate module for MRST. In this section, we verify and validate our upscaling strategy using three different test cases: The first is a simple box geometry, for which an analytical steady-state upscaling is available. The second case is a geologically realistic 3D stratigraphic model that will be upscaled to a single grid cell in a simulation model. The third case is an idealized 2D cross-section of a field-scale model.

Verification: Layered Model

To verify the upscaling methods, we consider a simple model of size (L_x, L_y, L_z) that consists of three stacked layers that are normal to the z-axis. The upper and the lower layers are of rock type one, while the middle layer is of rock type two. The model is depicted Figure 1.

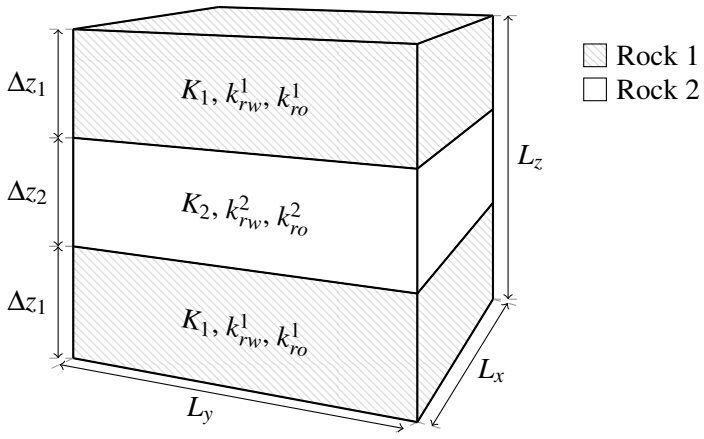

Figure 1: The simple layered model.

An analytic solution can be found if gravity and capillary pressure are neglected and we assume that both rock and fluid are incompressible and that the medium is homogeneous and isotropic. For the two-phase upscaling, it is further assumed that the relative-permeability curves are strictly monotonic functions of the phase saturations. Finally, we define functions for the arithmetic and harmonic average

$$A(K_1,K_2) = \frac{1}{L_z}\Big(2\Delta z_1 K_1 + \Delta z_2 K_2\Big), \quad H(K_1,K_2) = L_z\left(\frac{2\Delta z_1}{K_1} + \frac{\Delta z_2}{K_2}\right)^{-1}.$$

Using this notation, upscaled (absolute) permeability is found to be the diagonal matrix

$$K^* = \text{diag}(K^{*,x}, K^{*,y}, K^{*,z}), \quad \text{where} \quad K^{*,x} = K^{*,y} = A(K_1, K_2), \quad K^{*,z} = H(K_1, K_2).$$

The upscaled relative permeabilities for each phase $\alpha = \{o, w\}$ are given by

$$k_{r\alpha}^{*,d}(s_w^*) = A\Big(k_{r\alpha}^1(s_w)K_1, k_{r\alpha}^2(s_w)K_2\Big)\Big/K^{*,d}, \tag{9a}$$

for direction $d = \{x, y\}$, while for the z-direction, we have

$$k_{r\alpha}^{*,z}(s_w^*) = H\Big(k_{r\alpha}^1(s_w^1)K_1, k_{r\alpha}^2(s_w^2)K_2\Big)\Big/K^{*,d}. \tag{9b}$$

With flow in the x- or y-direction, parallel to the layers, the upscaled water saturation will equal the initial saturation, such that $s_w^* = s_w$. For flow in the z-direction, on the other hand, the water saturation s_w^1 in rock type one, will (in general) be different from s_w^2 in rock type two. These water saturations are found from the following expressions

$$\frac{k_{rw}^1(s_w^1)}{k_{ro}^1(s_w^1)} = \frac{k_{rw}^2(s_w^2)}{k_{ro}^2(s_w^2)}, \quad s_w^* = \frac{2s_w^1\Delta z_1 + s_w^2\Delta z_2}{2\Delta z_1 + \Delta z_2}.$$

It is possible to solve for s_w^1 and s_w^2 in these equations as we have assumed that the relative permeabilities are strictly monotonic functions.

Upscaling of the relative permeability factor R_k may also be computed analytically, by using the result that the steady-state polymer equations reduce to the two-phase problem (6), with altered relative permeability $\tilde{k}_{rw} = k_{rw}/R_k$. To find the upscaled R_k^*, we first upscale $\tilde{k}_{rw}$ using (9a) and (9b). Then, the upscaled relative permeability reduction factor is given by

$$R_k^{*,d}(s_w^*, c_p^*) = \frac{k_{rw}^{*,d}(s_w^*)}{\tilde{k}_{rw}^{*,d}(s_w^*)}, \qquad d = \{x, y, z\}.$$

The upscaled saturation s_w^* is the saturation from the upscaling of $\tilde{k}_{rw}^{*,d}$, and the upscaled concentration will be equal to the initial concentration, such that $c_p^* = c_p$.

As a specific example, we set the height of the layers equal, $\Delta z_1 = \Delta z_2$. The permeabilities of rock type one and two are set to 100 mD and 0.1 mD, respectively. The relative permeabilities of the two rocks are shown in Figure 2, together with the upscaled curves using flow-based upscaled. Likewise, Figure 3 shows the upscaled relative permeability reduction factors along with the original curves of the two rock types. For all curves, we see that there is a perfect match between the analytic and the numerical results. As expected, the R_k^* curves in the lateral directions do not depend on the average saturation. Moreover, we see that the relative permeabilities in the z-direction no longer have monotone derivatives.

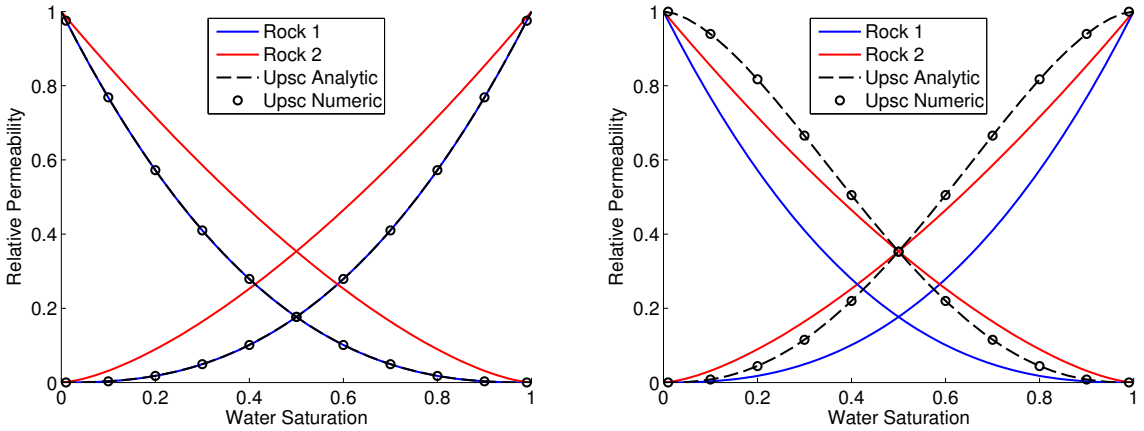

(a) x/y-direction (b) z-direction

Figure 2: Relative permeability curves for the simple layered model. The fine-scale curves are shown in blue for rock type one and red for rock type two. The dashed black lines are analytic upscaling, while circles denote numerical results using flow-based upscaling.

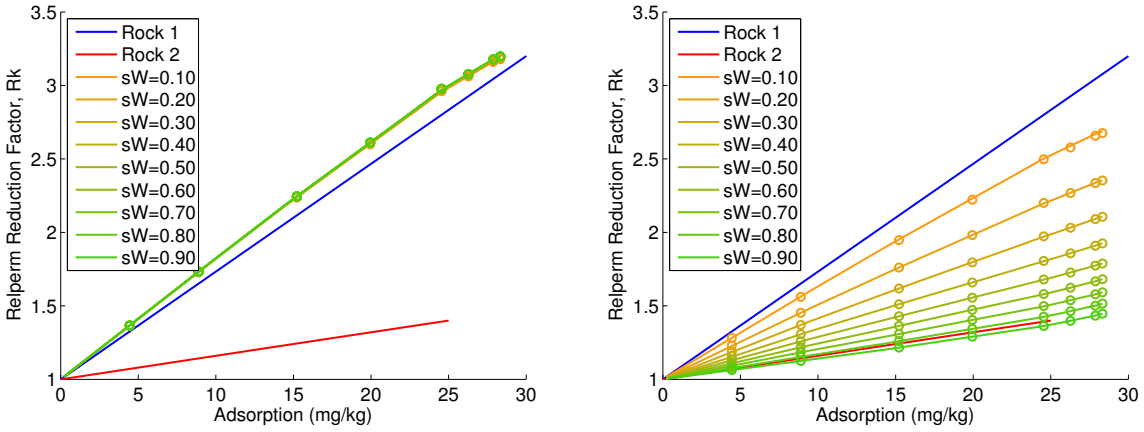

(a) x/y-direction (b) z-direction

Figure 3: Relative-permeability reduction factor R_k for the simple layered model. The fine-scale curves are shown in blue for rock type one and red for rock type two. The solid yellow-to-green lines are analyic upscaling, while the circles denote numerical results using flow-based upscaling. Note the water saturation dependency of R_k^* in the z-direction.

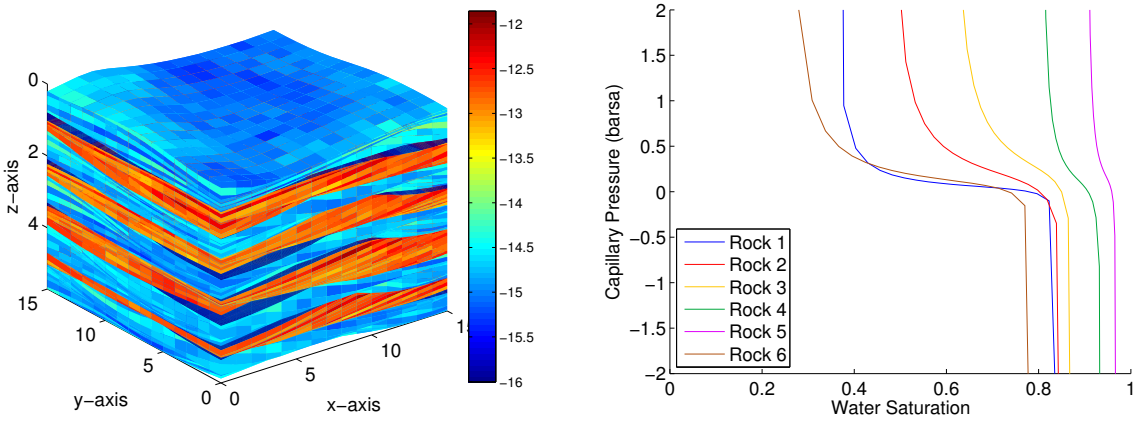

(a) Permeability

(b) Capillary pressure

Figure 4: (a) The permeability field of the SBED model shown on a log10 scale. The length unit of the grid is meters. (b) The capillary pressure curves of the different rock types.

Validation: SBED Model

As a validation of our method, we consider the upscaling of a high-resolution, core-scale model of realistic bedding structures to a single coarse block. So-called SBED models are geologically realistic stratigraphic models at sub-seismic scale (cm to meter) that define facies, bedding, and boundary patterns that impact fluid distribution. The models are used to propagate small-scale heterogeneities to large-scale models by proper (multiphase) upscaling procedures, thereby improving geological modeling (Lerdahl et al., 2005; Rustad et al., 2008). Over the past years, our group has developed multiphase, steady-state upscaling tools for SBED models. Figure 4a shows one such high-resolution model. The model has alternating layeres of high and low permeability, with a difference of approximately two orders of magnitude in the permeability between these layers. The model consists of six different rock types that each have their own relative permeability, capillary pressure, polymer adsorption, and residual resistance factor. Thus, each rock also has a different relative permeability reduction curve R_k. The capillary pressure curves for the different rock types are shown in Figure 4b.

We run the upscaling of this model in all three directions using the capillary and the viscous limit methods. The upscaled relative permeabilities are shown in Figure 5, together with the fine-scale curves for the six rock types. The upscaled reduction curves R_k are shown in Figure 6. Also here, the upscaled R_k depends on the water saturation, and in this case, we observe the R_k^* vary more with the water saturation in the viscous limit than in the capillary limit. Considering Figure 6c, it can be seen that R_k^* is not a monotonic function of water saturation for this particular upscaling.

Validation: Field-Scale Cross-Section

A particular challenge with simulating polymer flooding is that polymer fronts, unlike water fronts, are not self-sharpening and therefore highly susceptible to numerical diffusion. If the grid resolution is too low, a simulation will not be able to correctly predict the EOR effect of adding polymer because of the smearing and directional bias introduced by the numerical diffusion. In this last example, we will therefore try to shed some light into an important question for practical simulation: which error has the largest impact on the simulation quality – the upscaling error or the numerical diffusion introduced by going to a coarser grid?

The lateral resolution of a field-scale model will in many cases be approximately meters. As a conceptual model, we therefore consider the two-dimensional cross-section shown in Figure 7. The model is 2000 meters in the horizontal x-direction, and 10 meters in the vertical z-direction. The fine-scale grid consists

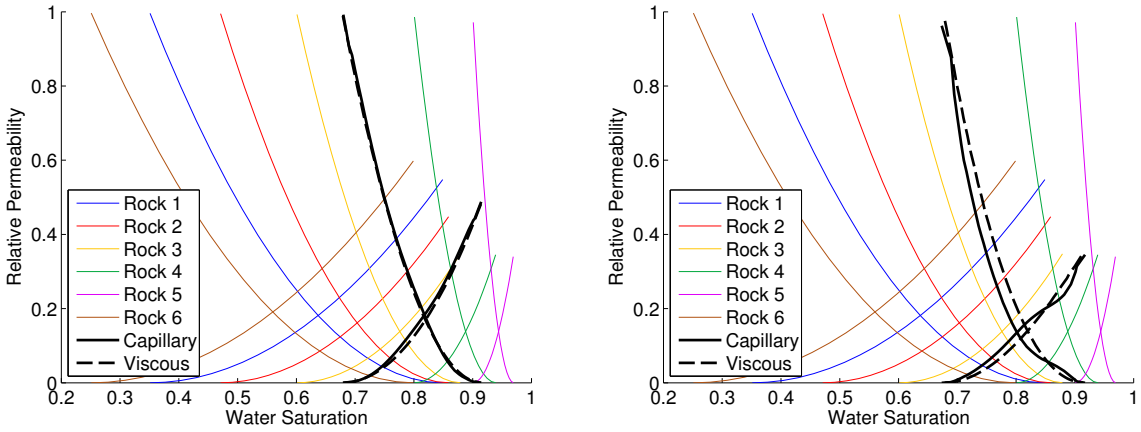

(a) x-direction (b) z-direction

Figure 5: Relative permeability upscaling for the SBED model. The y-direction is not shown, but the upscaling is almost identical to the x-upscaling.

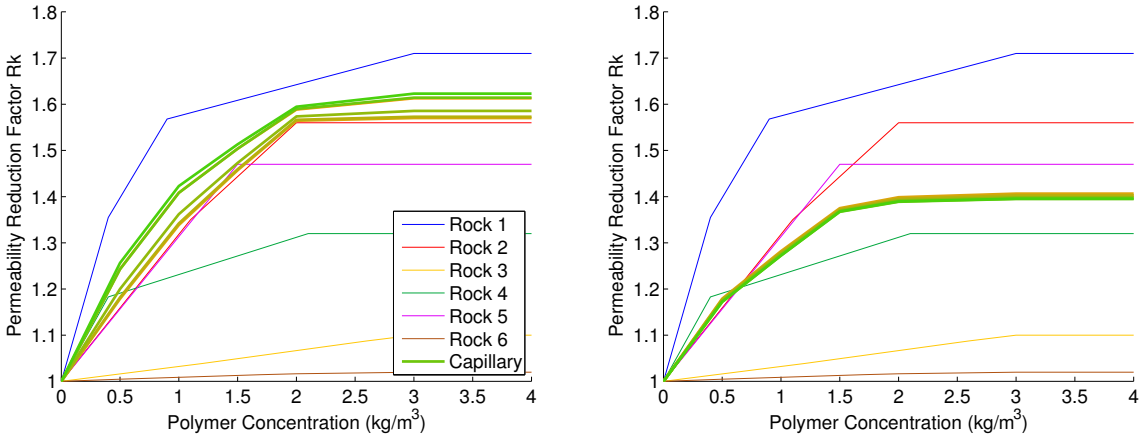

(a) Capillary limit, x-direction (b) Capillary limit, z-direction

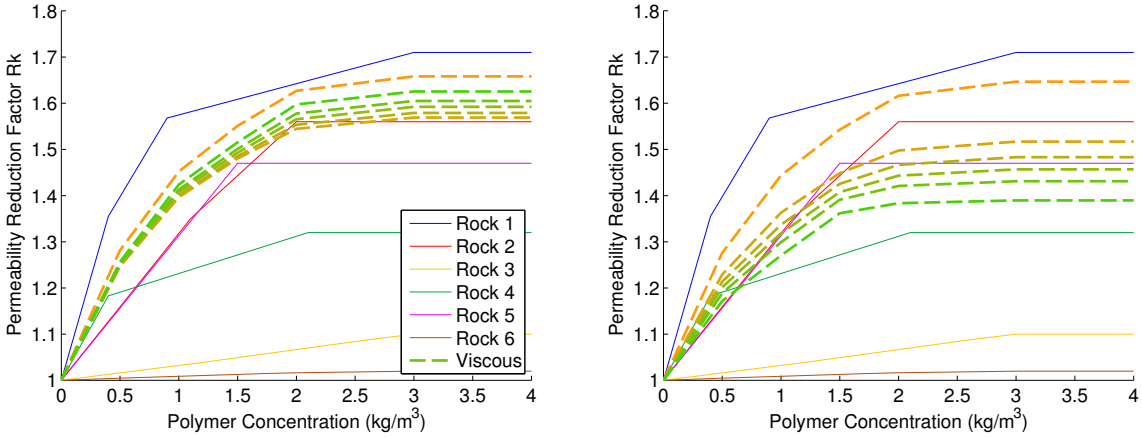

(c) Viscous limit, x-direction (d) Viscous limit, z-direction

Figure 6: Upscaling of the relative permeability reduction factor R_k for the SBED model. The fine-scale R_k curves for the six different rock types are also shown. The y-direction is not shown, but the upscaling is almost identical to the x-upscaling. The upscaled curves shown go from orange for the lowest s_w^* value, to green for the highest s_w^* values.

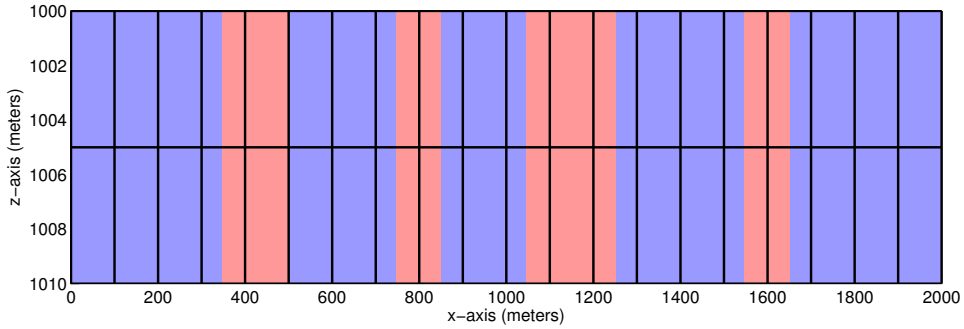

Figure 7: A conceptual model of a 2D cross-section from a field-scale model. The fine-scale rock types are shown in blue (rock type one), and in red (rock type two). The coarse grid blocks are shown on top with black lines.

of 400×10 cells, which we upscale to a uniform coarse grid of 20×2 cells. The model consists of two different rock types. Rock type one has a uniform permeability of 300 mD, and is shown in blue in Figure 7, while rock type two has a uniform permeability of 3 mD, and is shown in red. The two rock types also have different relative permeability cures, and different adsorption curves. The residual resistance factors are $\mathrm{RRF}_1 = 1.3$ and $\mathrm{RRF}_2 = 1.8$, respectively. The relative permeability curves and the reduction factor R_k are shown in Figure 9, together with the upscaled curves for one of the coarse grid blocks. The flow-based upscaling in this example is computed using periodic boundary conditions.

To compare the two sources of error, we will compare the result of three different simulation types: (i) simulation of the fine-scale model, (ii) simulation of the upscaled, coarse-scale model, and (iii) a fine-scale simulation using upscaled properties prolonged back to the original 400×20 grid. In all simulations, fluids are injected at a constant rate across the west boundary and extracted at the east boundary. First, pure water is injected, before a slug of polymer, followed by continued water injection.

To illustrate the characteristics of the solutions, Figure 8 shows the water saturation for the three different simulation types at the same time step. The coarse scale simulation is not able to capture the details of the solution, but the global picture is still seen to be similar to the fine scale simulation.

Figure 10 shows the flux across the east boundary computed by all three simulations with the mixing parameter set to $\omega = 1$ (full mixing) and $\omega = 0.8$ (partial mixing). Figures 10a and 10b show that the difference in results between the different upscaling methods is small compared to the difference between the fine and coarse-scale simulations. In particular, the production curves obtained by the viscous-limit and the flow-based methods are almost identical. Figures 10c and 10d show the fluxes obtained if we map the upscaled model back onto the fine grid. Compared with the coarse-scale simulations, we see that the error caused by the grid coarsening is much larger that the error caused by the upscaling of parameters. If the cross-section was part of a real model, our results would suggest that the best approach would be to use viscous-limit upscaling, which is significantly less expensive than the flow-based method, and try to increase the lateral resolution of the simulation model, e.g., by using techniques discussed by Lie et al. (2014).

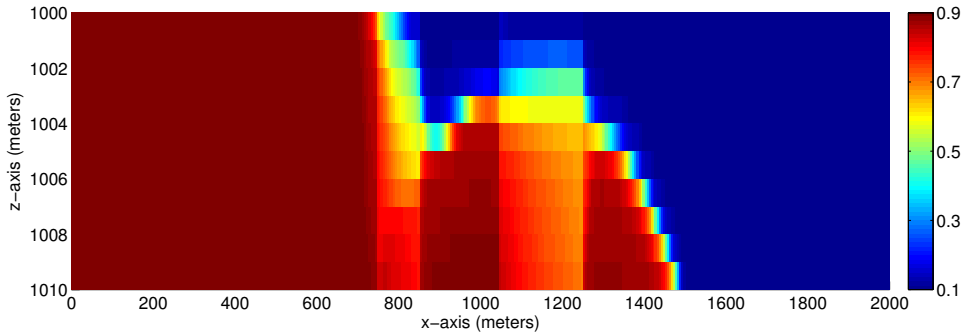

(a) Fine scale solution.

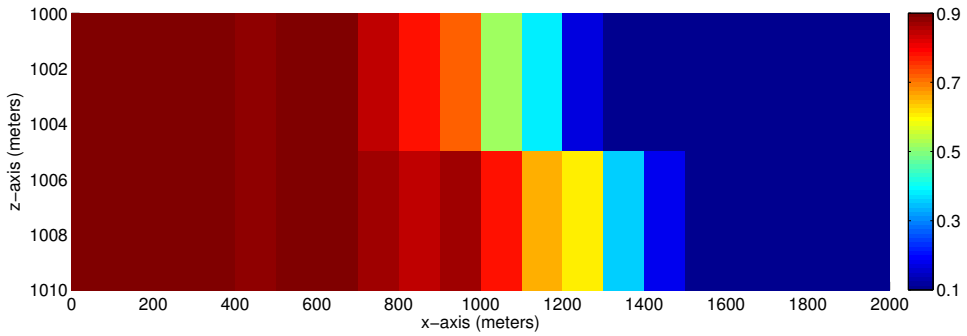

(b) Coarse scale solution with upscaled parameters.

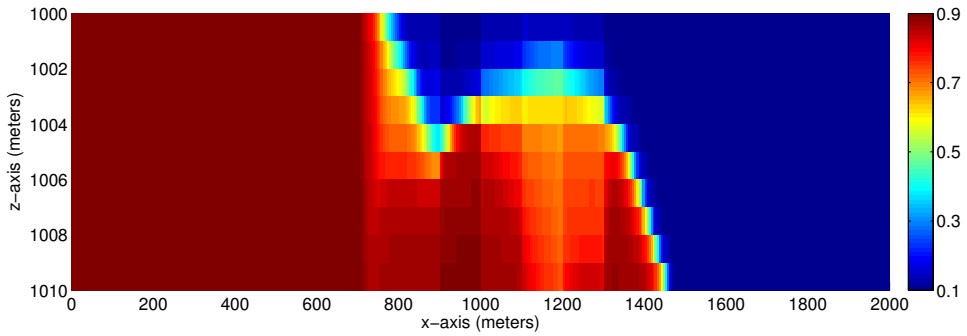

(c) Solution using upscaled parameters on the fine scale grid.

Figure 8: Water saturation for the field scale cross-section in the case where $\omega = 1$. The solution for the three different types of simulation considered are shown at the same simulation time.

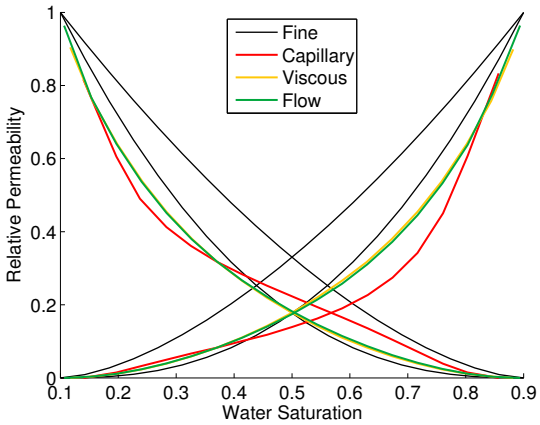

(a) Upscaled relative permeabilties in x-direction.

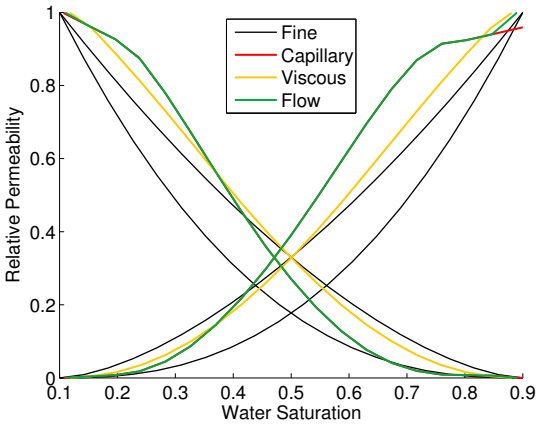

(b) Upscaled relative permeabilties in z-direction. The capillary and flow curves overlap.

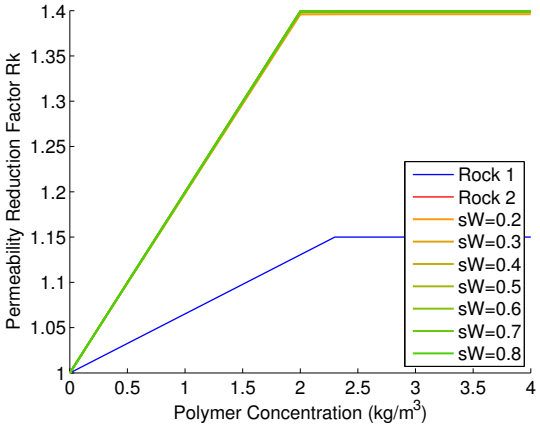

(c) Upscaled R_k using capillary limit, $\omega = 1$.

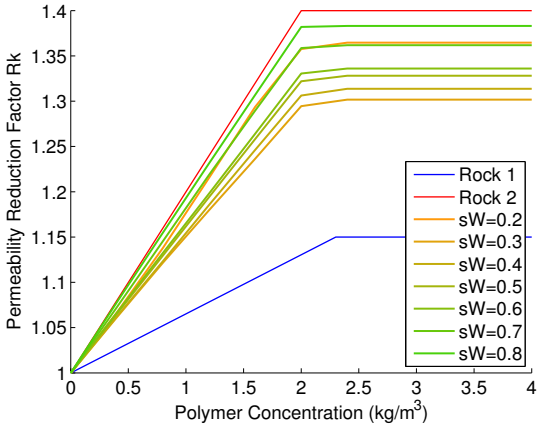

(d) Upscaled R_k using viscous limit, $\omega = 1$.

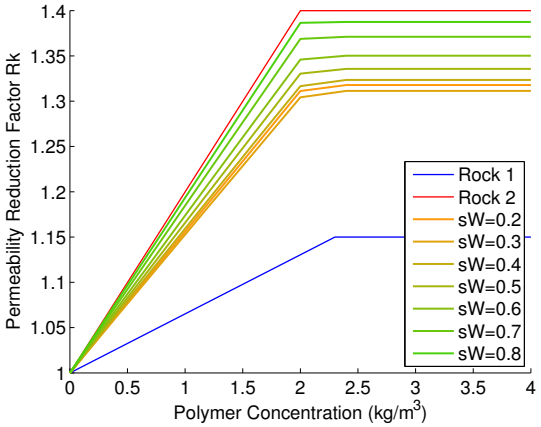

(e) Upscaled R_k using flow simulation, $\omega = 1$.

Figure 9: Upscaled curves for the field scale cross-section model. The curves are only shown for one of the coarse blocks where there are two different rock types on the fine scale.

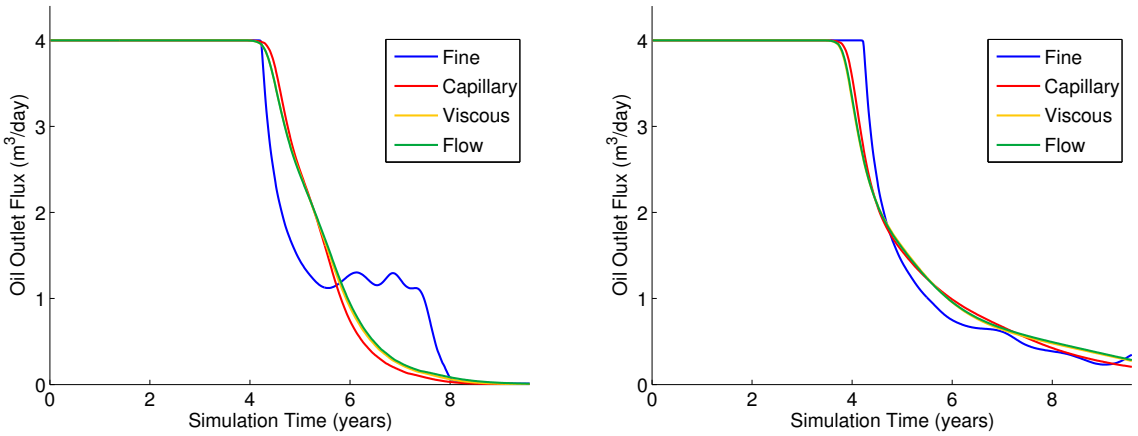

(a) Upscaling run on coarse grid, $\omega = 1.0$

(b) Upscaling run on coarse grid, $\omega = 0.8$

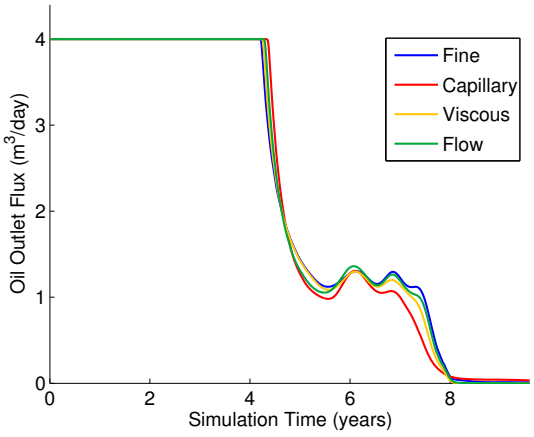

(c) Upscaling run on fine grid, $\omega = 1.0$

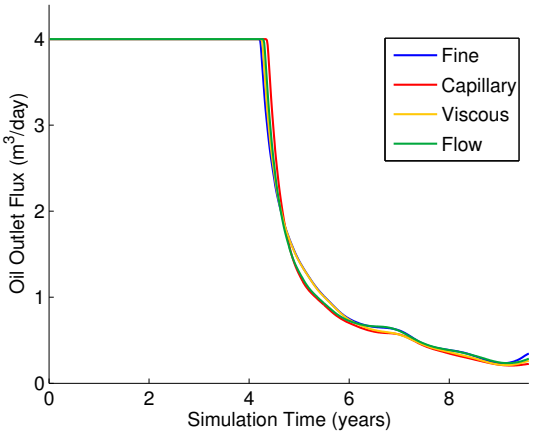

(d) Upscaling run on fine grid, $\omega = 0.8$

Figure 10: Solutions for the field scale cross-section model. The oil flux out of the east side boundary is shown (outlet flux). In the plots on top, upscaled parameters are used to run a simulation on the coarse grid. In the bottom plots, simulations are run on the fine scale grid using the upscaled parameters. In all plots, the fine-scale solution is shown in blue for comparison.

Concluding Remarks

In the paper, we have demonstrated how a framework for steady-state upscaling of two-phase flow can be extended to upscale the R_k factor that models permeability reduction in polymer flooding. In general, the upscaled values of R_k will depend on the water saturation in addition to the dependence on polymer concentration that is inherited from the underlying fine-scale model. This saturation dependency causes the amount of upscaled data to grow and introduces the need for lookup-tables and 2D interpolations in the coarse-scale simulation, which may potentially incur a high computational cost since R_k typically is evaluated multiple times for each time step. To reduce the computational complexity, one could consider fitting the upscaled R_k factors to a (nonlinear) parametric model.

From our preliminary experiments, we have also observed that the error introduced by coarsening the grid may dominate the upscaling error at the scale we are interested in (i.e., field-scale models with resolution of several tens to hundreds of meters). On one hand, this may indicate that it is possible to use simple analytical techniques (viscous or capillary limit upscaling) and hence avoid the cost of a flow-based method. On the other hand, the results also indicate that future research should focus on developing effective parameters that diminish the effects of numerical diffusion.

Finally, since the polymer concentration will be constant at steady state, it does not seem possible to use a steady-state method to upscale the mixing parameter ω. To be able to use this parameter to capture the effects of small-scale fingering induced by unresolved heterogeneity, one should look into alternative (dynamic) upscaling approaches.

Acknowledgments

The research is funded by VISTA, which is a basic research programme funded by Statoil and conducted in close collaboration with The Norwegian Academy of Science and Letters. The authors thank Statoil for providing data models, and Carl Fredrik Berg, Halvor Møll Nilsen, Olav Møyner, and Vegard Kippe, for helpful discussions.

References

Christie, M. [2001] Flow in porous media - scale up of multiphase flow. *Curr. Opin. Colloid Interface Sci.*, **6**(3), 236–241, doi:10.1016/S1359-0294(01)00087-5.

Lake, L.W. [2010] *Enhanced Oil Recovery*. Society of Petroleum Engineers.

Lerdahl, T.R. et al. [2005] Pore- to field scale multi-phase upscaling for ior. *SPE Europec/EAGE Annual Conference, 13-16 June, Madrid, Spain*, doi:10.2118/94191-MS.

Lie, K.A., Krogstad, S., Ligaarden, I.S., Natvig, J.R., Nilsen, H.M. and Skaflestad, B. [2012] Open source MATLAB implementation of consistent discretisations on complex grids. *Comput. Geosci.*, **16**, 297–322, ISSN 1420-0597, doi:10.1007/s10596-011-9244-4.

Lie, K.A., Nilsen, H.M., Rasmussen, A.F. and Raynaud, X. [2014] Fast simulation of polymer injection in heavy-oil reservoirs on the basis of topological sorting and sequential splitting. *SPE J.*, doi:http://dx.doi.org/10.2118/163599-PA.

MRST [2014] The MATLAB Reservoir Simulation Toolbox, v. 2014a. `http://www.sintef.no/MRST/`.

Pickup, G., Ringrose, P. and Sharif, A. [2000] Steady-state upscaling: From lamina-scale to full-field model. *SPE J.*, **5**(2), 208–217, doi:10.2118/62811-PA.

Rustad, A.B., Theting, T.G. and Held, R.J. [2008] Pore space estimation, upscaling and uncertainty modelling for multiphase properties. *SPE Symposium on Improved Oil Recovery, 20-23 April, Tulsa, Oklahoma, USA*, doi:10.2118/113005-MS.

Todd, M. and Longstaff, W. [1972] The development, testing, and application of a numerical simulator for predicting miscible flood performance. *J. Petrol. Technol.*, **24**(7), 874–882, doi:10.2118/3484-PA.